Design and validation of a multi-electrode embedded sensor to monitor resistivity profiles over depth in concrete

Joanna Badr, Yannick Fargier, Sergio Palma-Lopes, Fabrice Deby, Jean-Paul Balayssac, Sylvie Delepine-Lesoille, Louis-Marie Cottineau, Géraldine Villain

Design and Validation of a Multi-Electrode Embedded Sensor to Monitor Resistivity Profiles over Depth in Concrete

Joanna Badr [1, 2*], Yannick Fargier [2, 3], Sérgio Palma-Lopes [2], Fabrice Deby [1], Jean-Paul Balayssac [1], Sylvie Delepine-Lesoille [4], Louis-Marie Cottineau [2], Géraldine Villain [2]

1 LMDC, Université de Toulouse, INSA/UPS Génie Civil, Toulouse 31077, France;
badr@insa-toulouse.fr, balayssa@insa-toulouse.fr, f_deby@insa-toulouse.fr,
2 IFSTTAR, Site de Nantes, Bouguenais 44344, France; joanna.badr@ifsttar.fr,
geraldine.villain@ifsttar.fr, sergio.lopes@ifsttar.fr, louis-marie.cottineau@ifsttar.fr, Site de Bron,
Bron 69675, France; yannick.fargier@ifsttar.fr
3 CEREMA, Site de Blois, Blois 41029, France; yannick.fargier@cerema.fr
4 Andra, French National Radioactive Waste Management Agency, Chatenay-Malabry 92298,
France; Sylvie.Lesoille@andra.fr

*__Corresponding author__, e-mail address: badr@insa-toulouse.fr, joanna.badr@ifsttar.fr
Laboratoire Matériaux et Durabilité des Constructions de Toulouse LMDC, 135, Avenue de Rangueil, 31077 Toulouse Cedex 4, France.
Institut Français des Sciences et Technologies des Transports, de l'Aménagement et des Réseaux
IFSTTAR – Site de Nantes, MAST, LAMES, Allée des Ponts et Chaussées, CS4, F-44344 Bouguenais, France.

ABSTRACT

Electrical resistivity is sensitive to various properties of concrete, such as water content. Usually used on the surface of old structures, devices for measuring such properties could also be adapted in order to be embedded inside the constitutive concrete of the linings of new tunnels or in new bridges, to contribute to structural health monitoring. This paper introduces a novel multi-electrode embedded sensor for monitoring the resistivity profile over depth in order to quantify concrete durability. The paper focuses on the design of the sensor as a printed circuit board (PCB), which brings several advantages, including geometric accuracy and mitigation of wiring issues, thus reducing invasiveness. The study also presents the numerical modeling of the sensor electrical response and its ability to assess an imposed resistivity profile, together with experimental validations using (i) saline solutions of known conductivity and (ii) concrete specimens subjected to drying. The results demonstrate the capability of the sensor to evaluate resistivity profiles in concrete with centimeter resolution.

KEYWORDS

(Multi-electrode) embedded sensor; monitoring; electrical resistivity; concrete structures; finite element modeling.

1 INTRODUCTION

Water content is one of the main parameters governing the long-term durability of concrete structures. It is necessary to check hydric transfers over their entire thickness and not only in their concrete cover. Various methods enable concrete water content to be measured and monitored. They include Time Domain Reflectometry TDR [1–4], capacitive techniques [5–7], Ground Penetrating Radar GPR [8–10], electrical resistivity techniques [6,7,11–15] and Gammadensimetry [16,17] which is indirectly sensitive to the water content of concrete via its density. These different techniques have their own resolutions and constraints (related to the physical measurement but also to the signal processing). In this work, we specifically address the need to monitor the water content profile of concrete over its entire thickness. This is of great importance for the thick concrete repository structures used for radioactive wastes; and for applications that require a centimeter resolution over the entire thickness.

Surface measurement techniques are therefore excluded because their investigation depth typically does not exceed a few centimeters (e.g. attenuated signals, or effects of the reinforcement bed) and their resolution is intrinsically degraded with the depth. Moreover, for these same surface techniques, various problems (surface irregularities, material variability, segregation of aggregates, etc.) generate dispersion in measurements and penalize access to deeper information. Regarding the GPR technique, the surface measurements require a complex inversion procedure to assess hydric profiles [18–20] that may not yet be suitable for operational applications. As for the gammadensimetry

technique, it is restricted to test specimens and is not suitable for in situ structures. Thus, this study focuses on the development of an embedded sensor optimized as a multi-electrode system for monitoring resistivity profiles over depth. It takes advantage of the fact that resistivity is sensitive to defects [21] and to different concrete properties such as chloride penetration [22,23], corrosion [24] and concrete water content [6,7,13,25], which our study is centered on. Moreover, this new resistivity sensor is based on "point" electrodes, which give a suitable resolution for the targeted application.

The main aim of the work is to design a prototype of a sensor embedded in concrete structures to evaluate the resistivity profile over depth. The final goal is the evaluation of the water content profile. The transition from one to the other requires a conversion model (or calibration in the sense of [26]), which is dependent on the concrete mix design. The experimental determination of such conversion models is treated in the literature [6,7], and is outside the scope of the work reported here.

The paper starts with a general overview of the electrical resistivity principle, then the sensor and its originality (materials, geometry and measurement configurations) are presented, together with the associated methodology. Then the capabilities of the developed sensor are demonstrated and are validated by: 1) a numerical study, which shows that the approach (i.e. sensor with equi-distribution point electrodes) enables the resistivity profile to be estimated directly and 2) a twofold experimental campaign carried out on solutions of known conductivity and on concrete specimens. The latter results are then compared with independent reference measurements obtained by the gammadensimetry technique. Finally we discuss the results and conclude.

2 ELECTRICAL RESISTIVITY PRINCIPLE

A material's resistivity, expressed in Ω·m, is its ability to oppose the flow of an electric current. In concrete, the resistivity is characterized by the mobility of the ions existing in the interstitial solution

and influenced by the aqueous phase of the concrete. It is highly sensitive to the water content [6,13] and can be used as a performance parameter for concrete design [27]. A method for measuring the resistivity of a medium is the four point electrode method (quadrupole configuration) where the current is injected via two 'point' electrodes (C1 and C2) and the potential is measured between two other point electrodes (P1 and P2). By 'point' electrodes, we mean electrodes having dimensions that are smaller than one fifth of the minimum spacing between them [28]. It has been reported in previous studies that a four point measuring configuration yields more reliable results than a two-electrode system [6,29]. Different versions of the 4 point electrode method have been used as Non-Destructive Testing (NDT) methods, but, for applications concerning concrete, the Wenner configuration [30] is often used [6,7,31,32]. For this configuration, the electrodes are arranged in a line and are separated by a constant distance, the current is injected between the external electrodes and the potential drop is measured between the internal electrodes. A multi-electrode resistivity probe (multiple measurements usually based on a set of aligned and evenly spaced electrodes) can be used to perform electrical resistivity tomography (ERT) or to map property gradients over depth [6,23,24,33,34].

In the case of a homogeneous medium (including homogeneous water saturation conditions), the resistivity depends on the material and is connected to the resistance (ratio of measured voltage to injected current intensity) by a geometric factor G, which depends on the geometry of the quadrupole and the concrete structure under study. In the case of a heterogeneous medium, an "apparent" resistivity (ρ_a) is inferred from the same relation:

$$\rho_a = GR, \quad (1)$$

where R is the electric resistance measured in the heterogeneous medium.

95 The geometric factor G is calculated in a homogeneous medium having the same geometry and the
96 same electrode positions and combinations as the "real" experiment [35,36]:

$$G = \frac{\rho_0 I_0}{\Delta V_0}, \quad (2)$$

97 where ρ_0, ΔV_0 and I_0 are respectively the resistivity of the homogeneous medium, the measured
98 potential drop and the intensity of the electric current injected into the homogeneous medium.

99 3 DESIGN OF THE ELECTRICAL RESISTIVITY SENSOR

100 Our design was orientated by the many limitations described in previous studies regarding the
101 determination of the electrical resistivity profiles. Firstly, the problem of concrete monitoring over a
102 limited thickness (concrete cover) is counteracted by embedding a sensor in the concrete, thus
103 allowing centimeter resolution over the entire structure thickness. Secondly, the issue of invasive
104 cables in the concrete is resolved by the design of a Printed Circuit Board (PCB) sensor providing no
105 preferential path for water infiltration from the surface and offering good geometric accuracy of the
106 electrode shapes and positions. The third problem of the need to wet the surfaces of surface electrodes
107 to avoid loss of contact with the concrete [21] (which is not optimal for monitoring) is eliminated by
108 having our electrode embedded in the concrete. Moreover, to avoid the new risk of contact loss due to
109 concrete shrinkage, the design uses a specific shape.
110 We propose a printed circuit sensor as a possible solution that could meet all the needs and
111 requirements. The following subsections describe the design of the sensor and present its material,
112 geometry and measurement configurations.

113 3.1 Material

114 A PCB offers various advantages that make it a relevant choice for manufacturers of electronic
115 components and instruments: its low cost, its precision of fabrication, which is an important

parameter limiting any error due to an uncertainty on the electrode position or geometry that could impact the measurement [37] and, finally its compact thickness thanks to the interconnection between the components being made with copper tracks instead of using a large number of invasive cables, which enables a connection (such as DB25 connector) to be easily adapted to the measuring devices. For all these reasons, the use of PCB technology as a support for a resistivity probe looks promising. Regarding the support material, the PCB is based on a Flame Retardant-4 (FR-4) material, a glass-reinforced epoxy laminate [38]. All the physical (thermal expansion, resistivity), chemical and mechanical properties [https://en.wikipedia.org/wiki/FR-4] of the material make it a relevant choice, as pointed out by [38]. The conformal coating provides a dielectric layer on the probe that ensures good durability of the support and tracks.

Regarding the electrode material, the literature proposes a variety of materials that have been tested for geophysical applications [39], concrete [40,41] or metal applications [42]. The cost of the sensor is also an important parameter. It is kept down by, for instance, excluding platinum, which would not offer a significant improvement in signal stability compared to stainless steel [43]. Hence, the electrodes are made of copper plated with a nickel-gold layer, which has a low electrical resistivity [39] and protects against corrosion [44]. Alloyed with gold, nickel participates in the physical stability of the deposition layer and increases its hardness and mechanical resistance.

3.2 Geometry

The PCB sensor designed was given a ladder-like shape in order to ensure its anchoring in the concrete. One issue of concern was to prevent the PCB sensor itself from creating a preferential moisture flow path from the external DB25 connector (outlet of the copper tracks). It was therefore decided not to align the connector with the ladder axis but rather to shift it perpendicularly to the side

(Figure 1). Based on the hypothesis of unidirectional hydric transfer in semi-infinite structures (slabs, walls, etc.), only one-dimensional 1D resistivity profiles were assumed to be generated. This shape allows information to be obtained on the profile along the z axis, which is the direction of the gradient to be established. The PCB sensor consists of 19 electrodes, each having dimensions of 5x1.5 mm^2 staggered on either side of the circuit. The number of electrodes can evolve according to the thickness of the structure to be studied. The spacing between the electrodes is 2 cm on each side. The left and right hand side electrode lines in Figure 1 are shifted by 1 cm in the z-direction so that there is one electrode every centimeter in this direction, in order to increase the resolution through the depth.

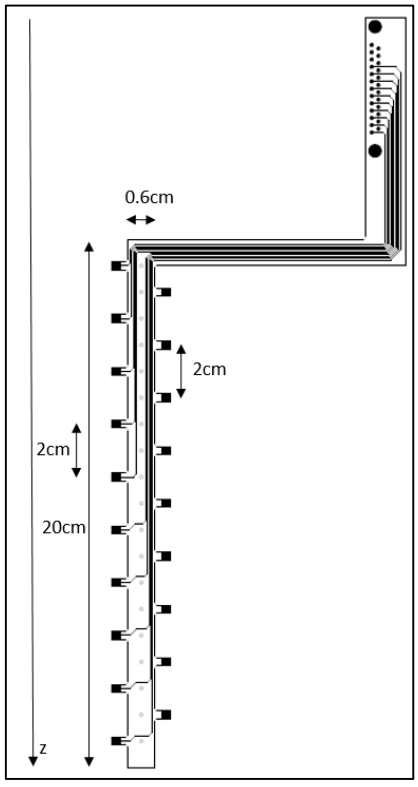

Figure 1. Schematic diagram of the ladder-shaped PCB sensor.

The PCB is placed between two stainless steel grids (Figures 2 and 3), each having a diameter of 100 mm and a thickness of 2 mm. The grids are used to focus the current lines in the zone determining the profile. For some measurement configurations (see section 3.3) this gives a finer resolution, as will be shown in the Numerical study section (section 4.1). The grids with 12 mm holes are designed

152 to facilitate the pouring of fresh concrete (assuming a maximum aggregate diameter D=12.5 mm) and
153 to enable water exchanges during drying and wetting processes.

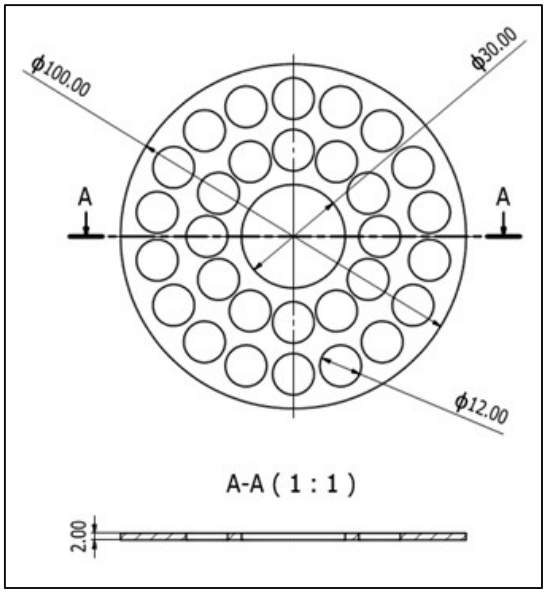

154

155 Figure 2. Schematic diagram of the stainless steel grid (dimensions in mm).

156 ### 3.3 Measurement Configurations

157 The ladder sensor presents two measurement configuration modes: the Transmission configuration,
158 in which the current is transmitted through the grids and the potential drops are measured between
159 electrode pairs, and the Wenner configuration, in which current injections and potential drop
160 measurements are made on the electrodes without using the grids.

161 For the Transmission configuration (Figure 3.a), the current, I, is injected by the two metal grids and
162 the potential difference (ΔV) is measured between two consecutive electrodes on the same side of the
163 sensor (P1 and P2 on Figure 3.a for instance, then P2 and P3, etc.). Thus we obtain nine apparent
164 resistivity measurements through the depth for the left side, and eight measurements for the right side.
165 For the Wenner configuration (Figure 3.b), four consecutive electrodes on the same side of the ladder
166 sensor are used: the current is injected on the external electrodes (C1 and C2) and the potential drop is

measured between the internal electrodes (P1 and P2). Thus we obtain seven apparent resistivity measurements along the left side, and six measurements on the right side.

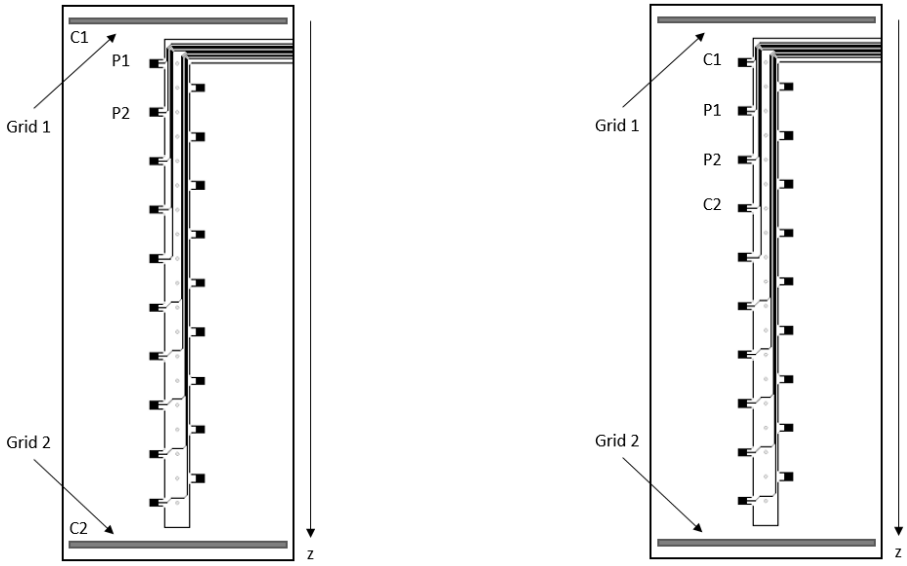

(**a**) (**b**)

Figure 3. Schematic diagram of the printed circuit configurations: (a) Transmission configuration; (b) Wenner configuration.

For both configurations, the depth of the resistance measurement is estimated at the middle of the electrodes where the potential is measured, as recommended by [45]. This assumption can be partly validated by the numerical modeling (section 4.1) and by a sensitivity calculation [46] which gives the sensitivity of a quadrupole to a small resistivity variation of its surrounding. This calculation is performed for both electrode measurement configurations, Wenner and Transmission. The approach of the "adjoint state method" [47] is used to compute the sensitivities here in a homogeneous medium (Figure 4). This kind of method, crucial during the inversion process, is often used to better understand and optimize a quadrupole measurement.

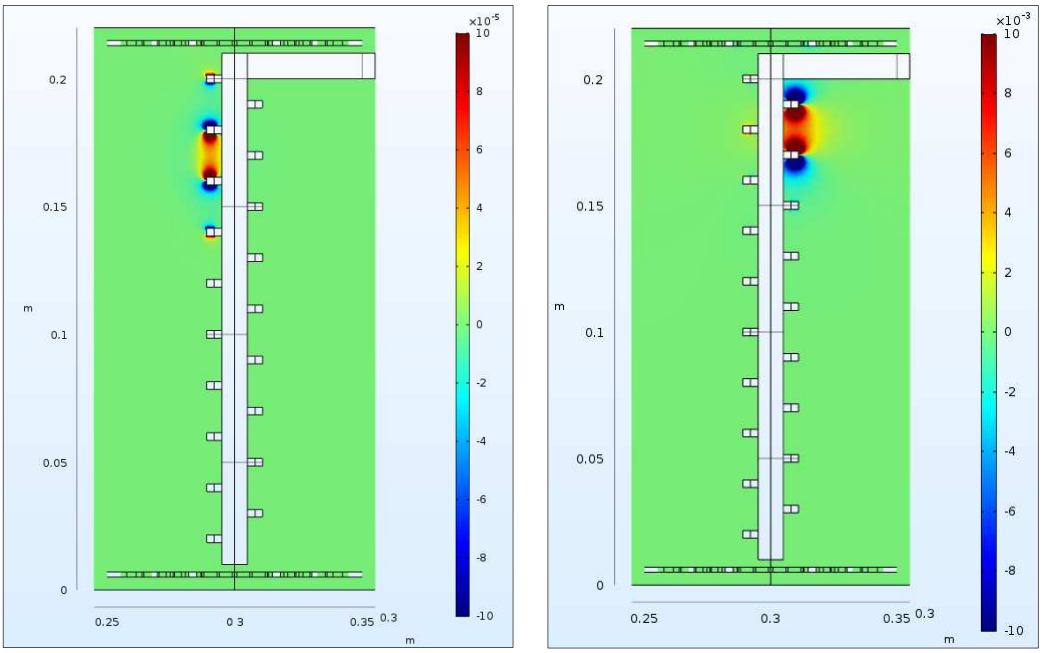

(a) **(b)**

Figure 4. Sensitivity calculation in a homogeneous medium: (a) Wenner configuration; (b) Transmission configuration.

As observed in Figure 4, all quadrupole measurements have zones of negative (blue) and positive (red) sensitivity. Concerning the Transmission configuration, results show that the measurement is not sensitive to the current electrodes C1 and C2.

4 VALIDATION OF THE MULTI-ELECTRODE RESISTIVITY SENSOR AND ASSOCIATED METHODOLOGY

In order to validate the PCB sensor, numerical modeling was carried out to test the sensor's response in a medium with an imposed resistivity profile defined to be representative of real situations in a concrete structure. In addition, the twofold experimental campaign comprised: i) tests in homogeneous brine solutions of known conductivity and ii) tests in concrete specimens to check the sensitivity of the resistivity measurements.

4.1 Numerical study

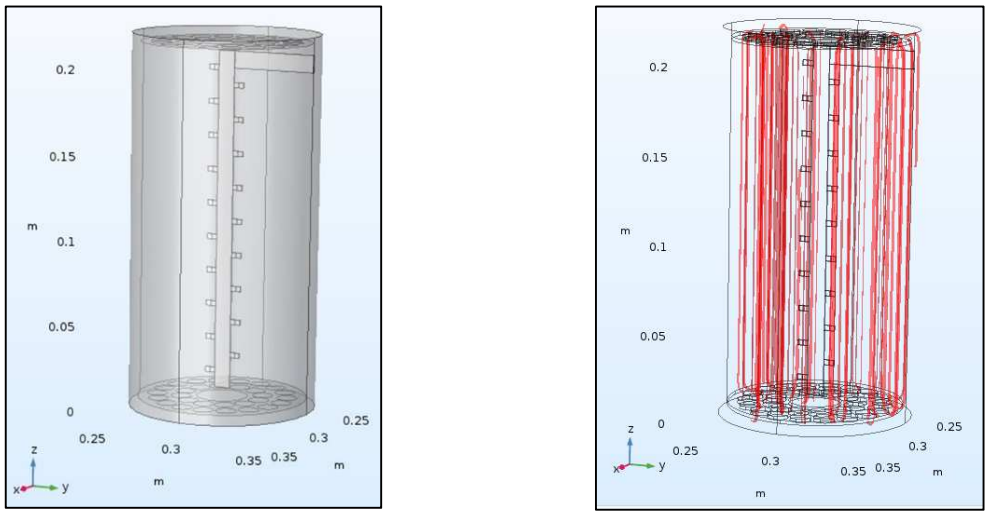

Figure 5. Numerical modeling of the response of the sensor to a known resistivity profile: (a) 3D view of the geometric model used for the sensor in a concrete specimen; (b) 3D view of some current lines in the Transmission configuration.

The goal of the numerical study was to demonstrate the relevance of the sensor geometry for 'capturing' resistivity profiles over the whole depth of a concrete element in a straightforward manner. The numerical simulation was conducted using a 3D electrostatic model and the AC/DC module integrated in COMSOL Multiphysics® (5.3 a), a commercial software based on the finite element method. We modeled the diffusion of the injected current using Poisson's equation (3) to find the electric potential scalar field, V, for a given resistivity distribution ρ. A very refined mesh was used, where the maximum dimension of the tetrahedral element was 0.5 mm. The boundary conditions were zero current flows on all boundaries to simulate perfect insulation.

$$\nabla\cdot(\frac{1}{\rho}\nabla V) = -I_s\delta(r - r_s), \tag{3}$$

where I_s is the current intensity in a point source S in r_s, δ a three-dimensional Dirac distribution and r the position of any point in space.

We modeled a cylindrical concrete specimen having a diameter of 11 cm and a length of 22 cm (standard specimen geometry). Two metallic grids (Figure 2) were embedded 5 mm from the plane

surfaces of the specimen. The PCB sensor was modeled and placed at the center of the cylinder, perpendicular to its end faces (representing the surfaces of a concrete structure) and therefore parallel to the direction of the resistivity profile to be retrieved (Figure 5.a). The shape and dimensions of the electrodes and grids were modeled with high precision identical to that of Figures 1 and 2. However, the electro-chemical and polarization phenomena at the interfaces between the concrete and the metallic parts of our sensor (electrodes and grids) were not taken into account [48]. The purpose was to test the sensor's response to a medium with an imposed resistivity profile.

The resistivity distribution was first considered constant (homogeneous concrete) in order to calculate the geometric factors G numerically and was then taken to be variable to study the profiles in depth. Thus, for each configuration and each quadrupole, a corresponding geometric factor, G, was obtained and an apparent resistivity, ρ_a, was calculated using equation (1).

The imposed resistivity profile was determined based on the range of electrical resistivity for different types of concrete [31]. For a CEM I Ordinary Portland Cement, depending on porosity, the resistivity varies between 30 and 200 Ω·m in humid conditions and between 100 and 400 Ω·m under natural conditions, without carbonation. It was estimated that this range of resistivity values would not be exceeded in the target application, the monitoring of concrete repository cells for radioactive wastes being similar, to that of concrete tunnels. Thus, in the numerical simulation, we propose an exponential resistivity variation between 400 Ω·m at the surface (z=0.22 m) and 50 Ω·m at depth (z=0), to obtain a higher decrease in the resistivity on the first half of the specimen than that at the heart. The imposed resistivity variation is given in equation (4):

$$\rho(z) = 350 \ \exp \ ((-13(0.22 - z))^3) + 50, \quad (4)$$

where ρ (Ω·m) and z (m) are the resistivity in the medium and the depth, respectively.

In the case of a Transmission configuration, current was injected between the two disk-shaped grids. This injection configuration generated current lines that were nearly parallel (i.e. approximately uniform electrical field (Figure 5.b)) between the grids, similarly to a cylindrical resistivity cell (e.g. [6]). This allowed a smaller volume to be investigated than for the Wenner configuration because this volume was more concentrated between the pair of electrodes used for the voltage drop measurement on the PCB sensor. Therefore we believe the Transmission configuration can achieve better accuracy and resolution, as is shown below.

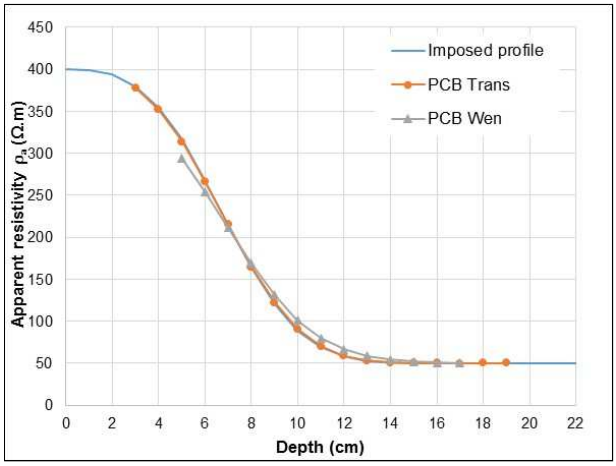

Figure 6. Simulated apparent resistivity profiles for the Transmission and Wenner configurations, compared to the imposed resistivity profile.

In order to compare the sensor's ability to match the resistivity profile imposed in the model (equation 3), we plotted the resistivity profile in Figure 6 as a function of depth for both the Transmission and the Wenner configurations. It is obvious from this figure that the relative difference between the actual resistivity distribution (imposed profile) and the simulated apparent resistivities is very small. The normalized mean root squared error (NRMSE) was calculated between the imposed profile and the calculated profiles of the PCB sensor. We found an NRMSE of 0.36% for the Transmission configuration, and 3.98% for the Wenner configuration. The greater difference observed for the Wenner configuration may be explained by the difference in the volume investigated

246 in the Wenner and the Transmission configurations. Therefore, with the Wenner configuration, a
247 numerical inversion procedure may be required to obtain the true resistivity profile [31]. However,
248 this promising result proves the ability of the designed sensor to determine the electrical resistivity
249 profile with good resolution for both configurations.

250 4.2 Experimental validation in brine solutions

251 The objective here was to assess the repeatability of the measurements, through laboratory
252 measurements acquired in homogeneous solutions (i.e. with negligible resistivity variation) in a range
253 of known conductivities. A measurement sequence for the Wenner and Transmission configurations
254 was programmed on a commercial resistivity meter (Syscal Pro, Iris Instruments) and all the
255 measurements were made automatically.

256 4.2.1 Experimental set up

257 The PCB sensor was placed at the center of a water-filled cubic tank of dimensions 30x30x30 cm^3
258 (Figure 7) between two stainless steel grids, each at a distance of 5 mm from the side surface. New
259 geometric factors were then calculated by a numerical simulation taking the new geometry of the
260 medium into account. The sensor was validated by testing various brine solutions of known resistivity
261 (the inverse of conductivity). To obtain the five solutions presented in Table 1, we gradually added
262 NaCl salt to demineralized water. The corresponding expected resistivity for each solution was
263 determined using Abacus software [49]. The values were then compared to those obtained by a
264 commercial conductivity probe (WTW Multi 348i), calibrated just before the measurements were
265 carried out. In addition, reproducibility tests performed with an internal quality control solution as
266 specified in standard XPT 90-220, based on inter-laboratory tests in which the French institute

267 IFSTTAR participated, evaluated the measurement uncertainty of the conductivity probe at 3%. The
268 experimental study was performed at a constant temperature of 20 ± 1 °C.

269 Table 1. Characteristics of the five electrolytes used.

	Solution 1	**Solution 2**	**Solution 3**	**Solution 4**	**Solution 5**
Concentration NaCl (mg/l)	10	50	90	200	1000
ρ expected (Ω·m)	(no value on the abacus)	100	63	25	5.5

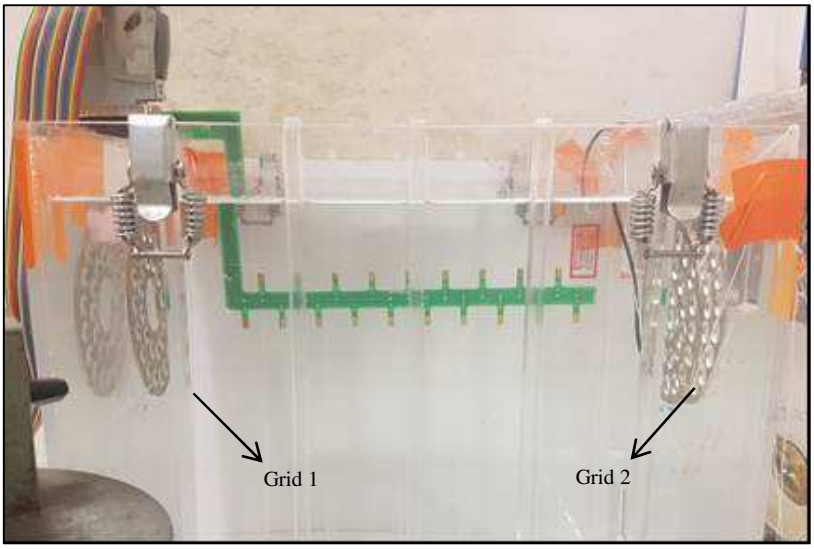

270

271 Figure 7. The PCB sensor and stainless steel grids tested in a brine solution.

272 **4.2.2 Results and discussion**

273 The repeatability was assessed by taking three measurements per quadrupole. Table 2 presents the
274 average and standard deviation of the resistivity measured with the PCB sensor in the Transmission
275 and Wenner configurations for all solutions. Solution 1, with low NaCl concentration, was excluded
276 since it had higher repeatability variation (1.7% for the Wenner configuration). The coefficient of
277 variation, CV, for the repeatability with solutions 2 to 5 varied from 0.2% to 0.6% and the CV for the
278 variability along the sensor line varied from 0.7% to 1.2%. All the results are detailed in Table 2.

279 Figure 8 presents the variation of the resistivity profiles over depth for the PCB sensor (Transmission
280 and Wenner configurations) and conductivity probe for solutions 2, 3, 4 and 5.
281 An average relative difference of 2.6% can be observed between the expected resistivity and that
282 measured with the conductivity probe. What is more, no significant degradation of the results over
283 time was observed that might have been associated with the change in the composition of the solution
284 by carbonation of the exchange surface.
285

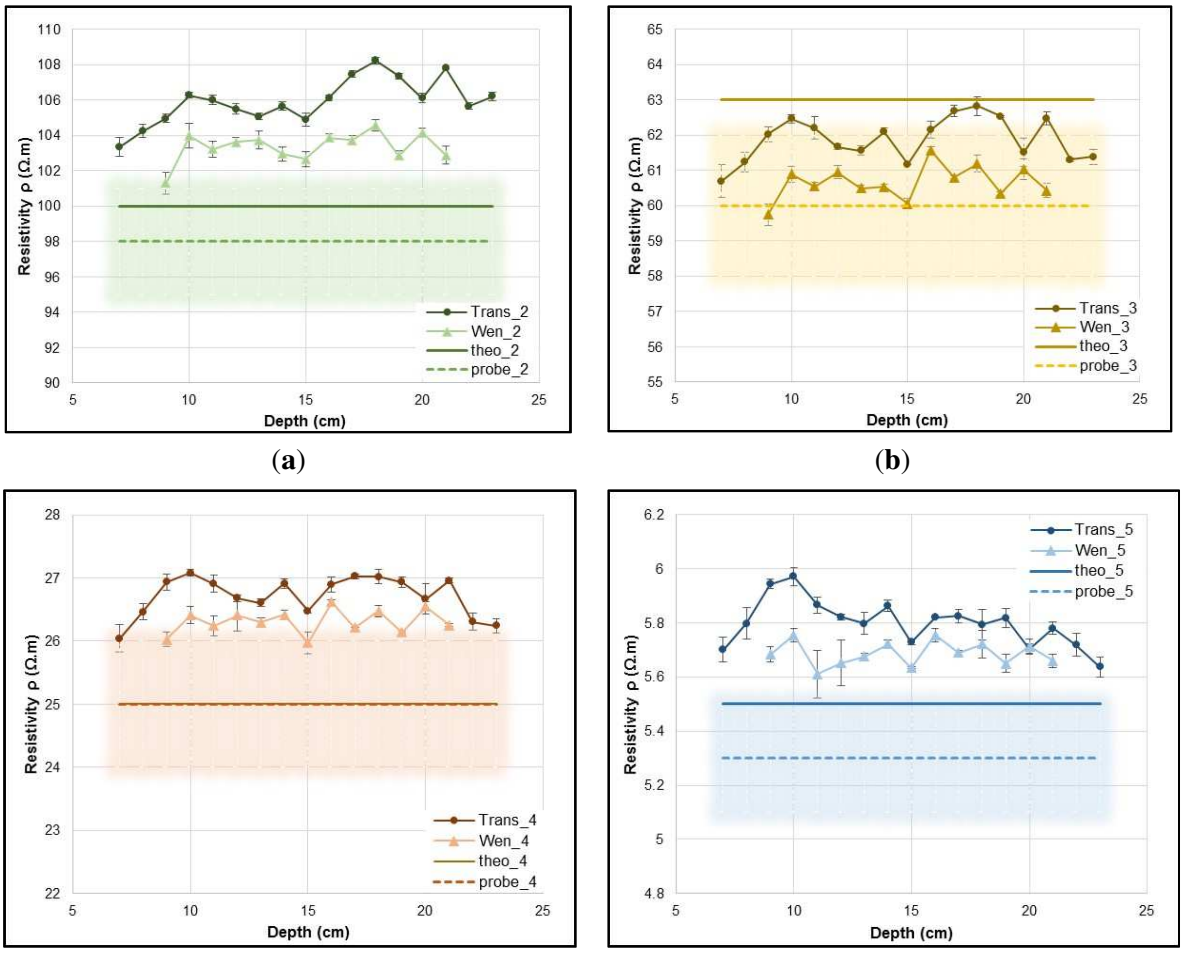

286 Figure 8. Variation of the resistivity profiles over depth for the PCB sensor (Transmission and Wenner
287 configurations) and the conductivity probe (uncertainty of the probe is highlighted): (a) solution 2; (b) solution
288 3; (c) solution 4; (d) solution 5.

289 Table 2. Electrical resistivity measured with the conductivity probe and the PCB sensor in the
290 Transmission and Wenner configurations for the five solutions.

	Solution 1	**Solution 2**	**Solution 3**	**Solution 4**	**Solution 5**
Conductivity probe ρ (Ω·m)	450 ± 13	98 ± 3	60 ± 2	25 ± 1	5.3 ± 0.2
PCB Trans ρ (Ω·m)	484.6 ± 1.4	105.9 ± 0.2	61.8 ± 0.2	26.7 ± 0.1	5.8 ± 0.03
CV repeatability (%)	0.3	0.2	0.3	0.4	0.5
CV variability (%)	2.9	1.2	1.0	1.2	1.5
PCB Wen ρ (Ω·m)	448.3 ± 7.4	103.4 ± 0.4	60.6 ± 0.2	26.3 ± 0.1	5.7 ± 0.03
CV repeatability (%)	1.7	0.4	0.3	0.4	0.6
CV variability (%)	1.0	0.8	0.8	0.7	0.8

291 The results in Table 2 and Figure 8 show that values for the resistivity measured with the PCB sensor
292 are in good agreement with the conductivity probe measurements; on average for all solutions, a

relative difference of 6.8% is calculated for the Transmission configuration and 4.8% for the Wenner configuration. Good correlation was found between measurements of the PCB sensor and the conductivity probe, as can be seen in Figure 9. These performances are equivalent to the state of the art [6] with surface measurements.

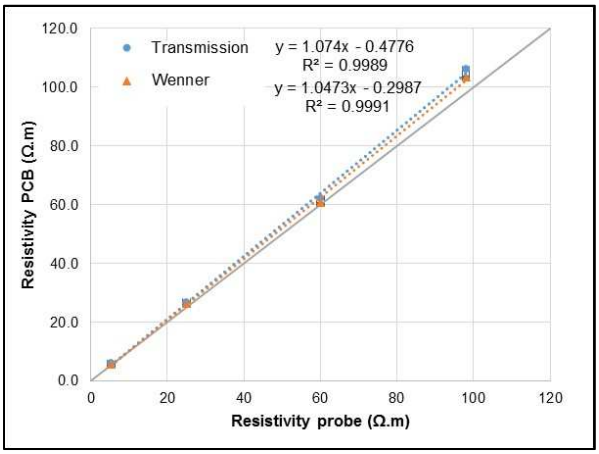

Figure 9. Correlation between the resistivity measured with the PCB sensor for the Wenner and Transmission configurations and the resistivity measured with the commercial probe.

4.3 Experimental validation in concrete specimen

This part of the study deals with the experimental validation of the sensor in a concrete specimen, the target material. We first demonstrate the ability to measure the concrete resistivity, then check the variability and repeatability of the measurements. In addition, the response of the sensor to concrete drying is studied. At the end of the experiments, a splitting tensile strength test was carried out on a specimen to visually check the contact between the electrodes and the concrete.

4.3.1 Experimental set up

The concrete used in this study was based on cement type 1 (CEM I) with a water-cement ratio of 0.59 and a porosity of 15.0% ± 0.9%. Five cylindrical specimens of diameter 11 cm and length 22 cm were used to quantify the variability of the measurement with the same sensor in all specimens. The PCB sensor was placed at the center of the cylinder and the grids (Figure 2) were placed on the external

311 surfaces of the mold, embedded in the concrete at a depth of 5 mm as in the numerical model (section
312 4.1). Tests were conducted after 28 days of curing, two concrete specimens were then dried at 20 °C
313 for 28 days, followed by drying at 45 °C to accelerate the establishment of a resistivity profile. The
314 cylinders were sealed with aluminum foil on the lateral and the underside faces; only the upper face
315 was kept in contact with the air to ensure a unidirectional drying. Conditions were thus close to the
316 drying conditions of a full-scale structure.

317 **4.3.2 Characterization of the sensor in concrete**

318 The repeatability assessment for the resistance measured over time showed a stable resistance value
319 for three measurements made 5 minutes apart in saturated conditions. The coefficient of variation
320 ranged between 0.07% and 1.86% for the Transmission configuration, and between 0.06% and 0.75%
321 for the Wenner configuration. In addition, the coefficient of variation CV for the variability along the
322 sensor line varied from 4.3% to 6.7% for the Transmission configuration, and from 2.5% to 5.7% for
323 the Wenner configuration.

324 To compare the Transmission and Wenner configurations, the apparent resistivity profiles for
325 cylinder 1 in saturated conditions are plotted in Figure 10. It can be observed that both configurations
326 have the same profile and follow similar trends (minima, maxima, changes of slope), which shows
327 that they are sensitive to the same parameters at each depth (state and variability of the concrete, state
328 of the contacts, etc.) although different apparent resistivity values ρ_a were measured. An NRMSE of
329 4.76% was calculated between the two configurations. This calls into question the initial idea of
330 estimating the depth of the resistance measurement at the middle of the electrodes, where the potential
331 is measured, especially for the Wenner configuration (see the numerical modeling in section 4.1).

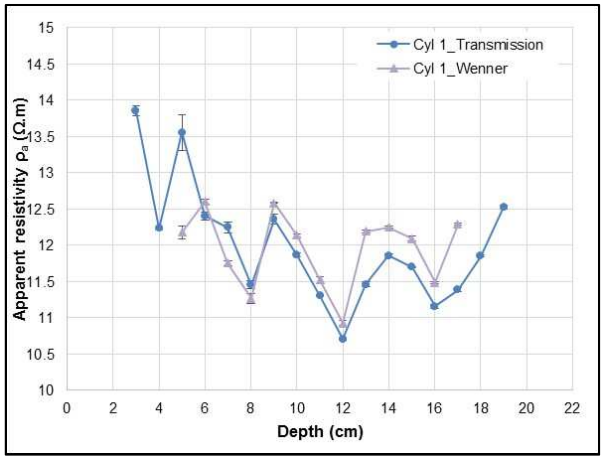

Figure 10. Apparent resistivity profile according to depth using the Transmission and Wenner configurations in saturated conditions for cylinder 1.

The reproducibility was assessed by testing the sensor's response variability in all cylindrical specimens subjected to the same laboratory conditions. The reproducibility here is associated with variation due to the sensor and concrete material variability. Figure 11 shows the variation of the apparent resistivity profile with depth for all specimens, using the Transmission configuration in saturated conditions. The apparent relative variation of resistivity is 4.6% on average between cylinders 1, 3, 4 and 5, and 11.1% for all cylinders including cylinder 2, which has higher resistivity values. These ranges of CV for the reproducibility measurements in concrete are similar to those reported by Morris [50] (4% to 11%) with a surface Wenner probe in saturated conditions. According to Andrade et al. [32], a CV of 10% is good and 20% is acceptable for controlled conditions, while up to 30% is normal for on-site conditions.

Therefore, for this case study, it can be concluded that the PCB sensor developed yields results within an acceptable range of variability.

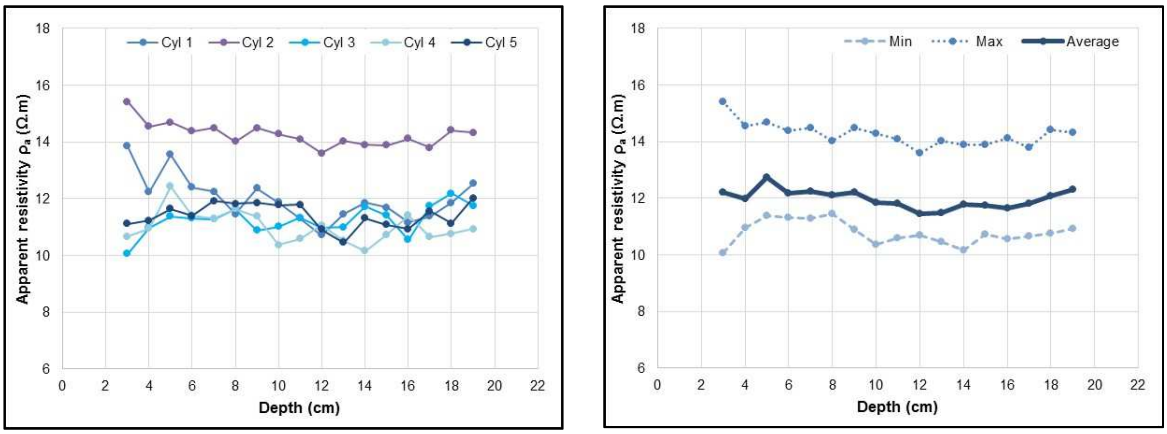

(**a**) (**b**)

Figure 11. Apparent resistivity profile over depth using the Transmission configuration in saturated conditions: (a) all cylinders; (b) average profile with the minimum and maximum profiles.

In order to test the sensitivity of the sensor to drying, the variation of the apparent resistivity profile with time is illustrated in Figure 12 for the Transmission configuration, where t0 marks the beginning of concrete drying at 20 °C and t'0 marks the beginning of concrete drying at 45 °C. In Figure 12, the relative apparent resistivity variation $\Delta\rho_a$ for each depth was calculated relative to a reference time using equation 5:

$$\Delta\rho_a = \frac{\rho_t - \rho_{0ref}}{\rho_{0ref}} \quad (5)$$

where ρ_t is the apparent resisitivity value at a time t and ρ_{0ref} is the apparent resisitivity value measured at the beginning of each drying process (t0 in Figure 12.a and t'0 in Figure 12.b respectively).

The measured apparent resistivity shows a general increase over time, which implies a decrease of the water content due to the drying process. The water content profile created between the two faces of the cylinder is caused by the evaporation of the water from the face that is in contact with the air. We observe in Figure 12 that the relative apparent resistivity variation near the surface is higher than that at the heart. This is due to the unidirectional drying of the concrete. Similar tendencies have been observed in previous studies concerning the determination of water content gradients, such as

363 [7,13,14]. In addition, when the drying was accelerated at 45 °C (Figure 12.b), the relative apparent
364 resistivity variation increased more rapidly near the surface. This demonstrates the ability of the
365 designed sensor to monitor the resistivity profile due to concrete drying with a spatial resolution of
366 about 1cm.

367 For very low degrees of saturation (less than 30–40% according to Lataste et al. in [12], even 20-30%
368 for certain concrete mixes), the hydric continuity is not sufficient in the porosity and the resistivity
369 becomes too high (between 2000 and 4000 Ω·m) to be measured by available commercial resistivity
370 meters. However, in the study presented herein, such very low degrees of saturation have not yet been
371 reached after 2 years of drying in conditions corresponding to thick concrete structures.

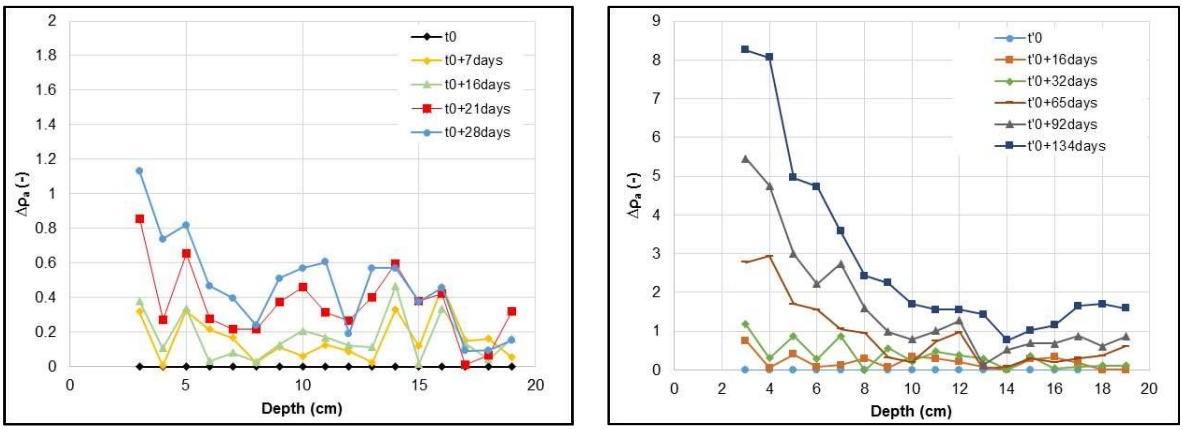

(**a**) (**b**)

372 Figure 12. Relative apparent resistivity variation profile over depth using the Transmission configuration
373 during the drying of the concrete specimen: (a) at 20 °C; (b) at 45 °C.

374 **4.3.3 Visual check of the contact between electrodes and concrete**

375 A splitting tensile strength test was carried out on one concrete specimen to visually verify the contact
376 between the PCB sensor electrodes and the concrete. Figure 13 shows a photograph of the splitting of
377 the concrete specimen with a close-up on the electrodes and their footprints left in the concrete.

378 Good contact is observed between all electrodes (PCB electrodes and grids) and the concrete,
379 verifying the adhesion between the concrete and the PCB sensor, which does not present any sign of

alteration. The aggregates were able to penetrate between two consecutive electrodes and to pass through the grids well (previous assumption). The contact resistances measured between pairs of electrodes varied from 7 kΩ (beginning of drying) to 35 kΩ (end of drying), and from 2 kΩ (beginning of drying) to 10 kΩ (end of drying) on the grids. The influence of the PCB sensor on the concrete strength can be considered as minimal in the application of the thick concrete repository structures used for radioactive wastes since the volume of the sensor is small compared to the global volume of the structure.

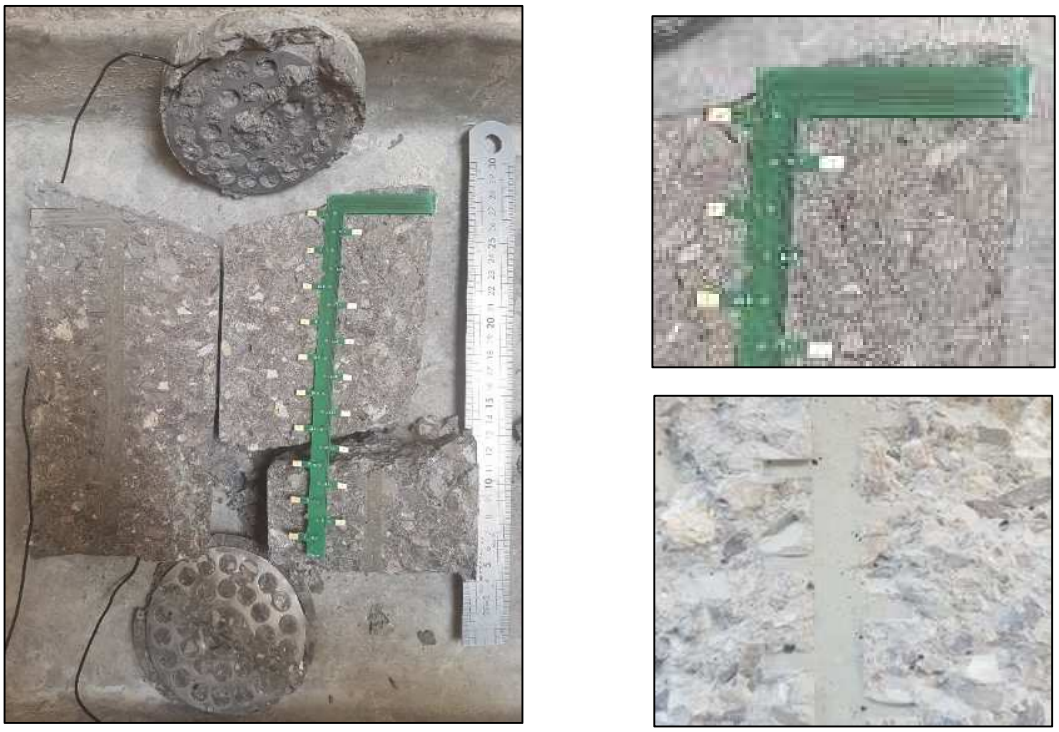

(**a**) (**b**)

Figure 13. Photos of the split concrete specimen: (a) general view of the PCB sensor and the grids; (b) close-up on the electrodes (top) and their footprints in the concrete (bottom).

5 VALIDATION WITH GAMMADENSIMETRY DATA AND DISCUSSION

Gammadensimetry is a method commonly used to check concrete density [16,17]. It is also used to determine water content profiles. By taking the water loss into account in the calculation of the mass absorption coefficient, the accuracy of the parameter characterizing the concrete internal water content is improved [16]. It is based on the material's absorption of gamma rays emitted by a Cesium

137 radioactive source. The diameter of the test specimen used here was 11cm and its height was 30 cm. It was sealed with aluminium foil and exposed to drying conditions similar to those of the cylindrical specimens where the PCB resistivity sensor was embedded. It was placed with a rotational movement about its axis: the measurement corresponded to the average over a slice of concrete having an estimated thickness of 10 mm. One measurement was made every 6 mm. The uncertainty of gammadensimetry values is estimated at 0.5%. We calculated the relative density variations for each depth and each time in both drying processes (at 20 °C and 45 °C) relative to an initial state (reference time) using a simple expression (similar to Eq. (5)). The results are plotted in Figure 14, where T0 marks the initial saturated state and the beginning of concrete drying at 20 °C and T'0=T0+146 days marks the beginning of concrete drying at 45 °C.

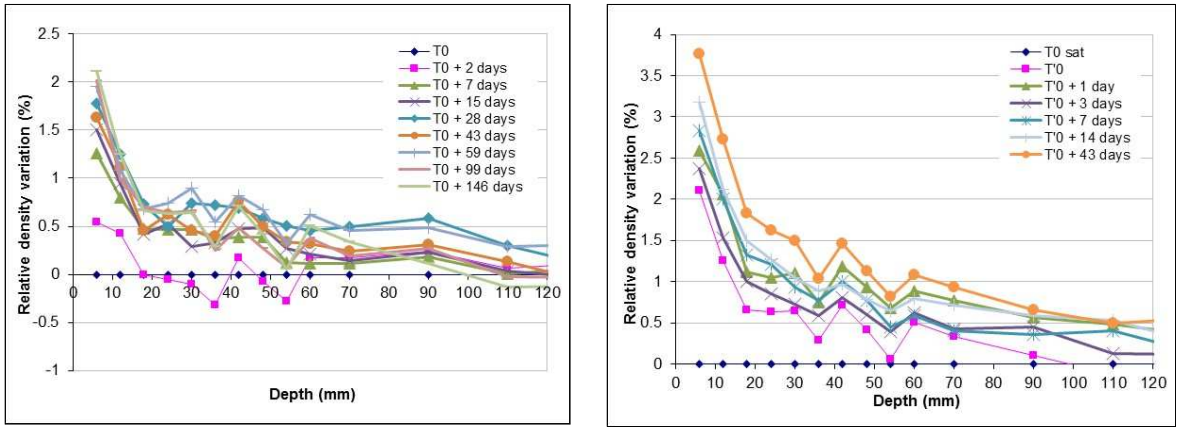

(**a**) (**b**)

Figure 14. Relative density variation over depth during the drying of the concrete specimens: (a) at 20 °C; (b) at 45 °C.

An increase in the relative density variation is observed over time, revealing the drying of the concrete. The relative density variation on the surface at 20 °C is equal to 0.6% for t0+2 days and 2.3% for t0+146 days. At 45 °C, the relative density on the surface varies between 2.3% and 3.8% over 42 days. The concrete took a very long time to dry even after the temperature increase. To make a comparison between the relative density and apparent resistivity variations (using the Transmission

411 configuration) with depth, Figure 15 shows both variations plotted on the same graph for certain
412 common times within the drying process.
413

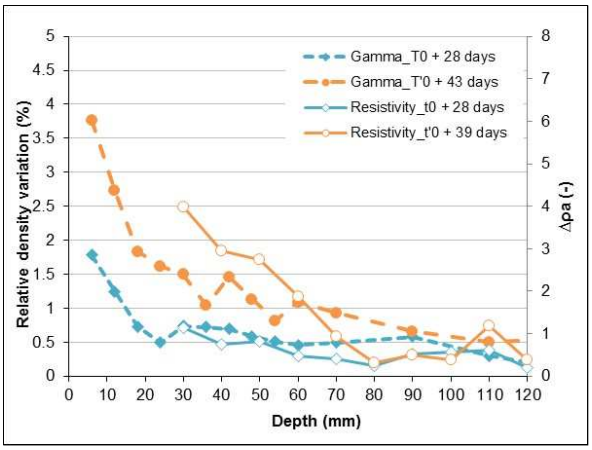

414
415 Figure 15. Relative density (left axis) and apparent resistivity (right axis) variations over the concrete
416 specimen depth.

417 Gammadensimetry makes it possible to monitor the drying of the concrete [16] and correlates well
418 with the relative apparent resistivity variation profiles over time. Similar variations can also be
419 observed in Figure 15 for the density and apparent resistivity measured in the concrete. According to
420 our results, the PCB sensor sensitivity varies from 10 to 40 ± 10 Ω·m for a saturation degree variation
421 from 100 to 73 ± 5% (calculated by gammadensimetry). Considering results given in the literature
422 [6,7] and Archie's law [51], the sensitivity range should be higher for lower saturation degrees, when
423 the drying is at an advanced stage. Therefore, further research should include long-term drying to
424 achieve lower saturation degrees and extend our results.

425 ## 6 CONCLUSIONS

426 In this paper, a PCB sensor based on an electrical resistivity technique has been developed to evaluate
427 the resistivity profile in concrete in order to monitor moisture gradients in real structures. The
428 embedded sensor presents various advantages, such as measuring profiles at the centimeter scale over

429 the thickness of a concrete structure; ensuring good electrical contacts between the electrodes and the
430 concrete, which is optimal for monitoring purposes; having good precision and low fabrication cost
431 and reducing the handling of wiring. A numerical study was conducted to validate the sensor's
432 response. Results show that apparent resistivity profiles simulated for the Transmission and Wenner
433 configurations are quite close to the actual resistivity profile. Experimental measurements were
434 carried out on electrolytes of known conductivities and the sensor proved its ability to determine
435 resistivity values accurately. Moreover, a validation of the PCB sensor was carried out on concrete
436 cylindrical specimens and the apparent resistivity profile was monitored at different times of drying.
437 The apparent resistivity data were shown to be sensitive to the evolution of concrete while it was
438 drying over time. The results are validated by comparison with independently measured
439 gammadensimetry data. In the future, we plan to optimize the measurement configurations using the
440 sensitivity study. The PCB sensor may be used in many structures to monitor resistivity profiles and,
441 more importantly, moisture content profiles by means of material-dependent calibration.

442 **Acknowledgments:** The authors are grateful to Jean-Luc Geffard from the Materials and Structures
443 department in IFSTTAR and Carole Soula from the Laboratory of Materials and Durability of
444 Constructions (LMDC) for the technical support they provided. Our thanks are extended to Susan
445 Becker, a native English speaker, commissioned to proofread the final English version of this paper.

446 **References**

447 [1] T. Bore, N. Wagner, S. Delepine Lesoille, F. Taillade, G. Six, F. Daout, D. Placko, Error
448 Analysis of Clay-Rock Water Content Estimation with Broadband High-Frequency
449 Electromagnetic Sensors—Air Gap Effect, Sensors. 16 (2016) 554. doi:10.3390/s16040554.
450 [2] R. Farhoud, J. Bertrand, S. Buschaert, S. Delepine-Lesoille, G. Hermand, Full scale in situ
451 monitoring section test in the Andra's Underground Research Laboratory, in: Proceedings of
452 the 1st Conference on Technological Innovations in Nuclear Civil Engineering (TINCE), Paris,
453 France, 2013: pp. 29–31.

[3] A. Courtois, T. Clauzon, F. Taillade, G. Martin, Water Content Monitoring for Flamanville 3 EPR TM Prestressed Concrete Containment: an Application for TDR Techniques, (2015).
[4] S. Arsoy, M. Ozgur, E. Keskin, C. Yilmaz, Enhancing TDR based water content measurements by ANN in sandy soils, Geoderma. 195 (2013) 133–144.
[5] X. Dérobert, J. Iaquinta, G. Klysz, J.-P. Balayssac, Use of capacitive and GPR techniques for the non-destructive evaluation of cover concrete, NDT & E International. 41 (2008) 44–52.
[6] R. Du Plooy, S.P. Lopes, G. Villain, X. Derobert, Development of a multi-ring resistivity cell and multi-electrode resistivity probe for investigation of cover concrete condition, NDT & E International. 54 (2013) 27–36.
[7] M. Fares, G. Villain, Y. Fargier, M. Thiery, X. Derobert, S. Palma-Lopes, Estimation of water gradient and concrete durability indicators using capacitive and electrical probes, in: NDT-CE 2015, International Symposium Non-Destructive Testing in Civil Engineering, 2015: p. 9p.
[8] Z.M. Sbartaï, S. Laurens, J. Rhazi, J.P. Balayssac, G. Arliguie, Using radar direct wave for concrete condition assessment: Correlation with electrical resistivity, Journal of Applied Geophysics. 62 (2007) 361–374.
[9] A. Ihamouten, G. Villain, X. Derobert, Complex permittivity frequency variations from multioffset GPR data: Hydraulic concrete characterization, IEEE Transactions on Instrumentation and Measurement. 61 (2012) 1636–1648.
[10] İ. Kaplanvural, E. Pekşen, K. Özkap, Volumetric water content estimation of C-30 concrete using GPR, Construction and Building Materials. 166 (2018) 141–146.
[11] S.G. Millard, Reinforced concrete resistivity measurement techniques, in: Institution of Civil Engineers, Proceedings, 1991.
[12] J.-P. Balayssac, V. Garnier, Non-destructive testing and evaluation of civil engineering structures, Elsevier, 2017.
[13] G. Villain, Z.M. Sbartaï, J.-F. Lataste, V. Garnier, X. Dérobert, O. Abraham, S. Bonnet, J.-P. Balayssac, N.T. Nguyen, M. Fares, Characterization of water gradients in concrete by complementary NDT methods, in: International Symposium Non-Destructive Testing in Civil Engineering (NDT-CE 2015), 2015: p. 12p.
[14] J.-P. Balayssac, V. Garnier, G. Villain, Z.-M. Sbartaï, X. Dérobert, B. Piwakowski, D. Breysse, J. Salin, An overview of 15 years of French collaborative projects for the characterization of concrete properties by combining NDT methods, in: Proceedings of Int. Symp. on NDT-CE, 2015: pp. 15–17.
[15] H. Minagawa, S. Miyamoto, M. Hisada, Relationship of Apparent Electrical Resistivity Measured by Four-Probe Method with Water Content Distribution in Concrete, Journal of Advanced Concrete Technology. 15 (2017) 278–289.
[16] G. Villain, M. Thiery, Gammadensimetry: A method to determine drying and carbonation profiles in concrete, Ndt & E International. 39 (2006) 328–337.
[17] G. Villain, M. Thiery, G. Platret, Measurement methods of carbonation profiles in concrete: Thermogravimetry, chemical analysis and gammadensimetry, Cement and Concrete Research. 37 (2007) 1182–1192. doi:10.1016/j.cemconres.2007.04.015.
[18] M. Albrand, G. Klysz, X. Ferrieres, P. Millot, Evaluation of the electromagnetic properties of non-homogeneous concrete by inversion of GPR measurements, in: 2016 16th International Conference on Ground Penetrating Radar (GPR), Ieee, Hong-Kong, 2016: pp. 1–4.

[19] X. Xiao, A. Ihamouten, G. Villain, X. Dérobert, Use of electromagnetic two-layer wave-guided propagation in the GPR frequency range to characterize water transfer in concrete, NDT & E International. 86 (2017) 164–174. doi:10.1016/j.ndteint.2016.08.001.

[20] B. Guan, A. Ihamouten, X. Dérobert, D. Guilbert, S. Lambot, G. Villain, Near-Field Full-Waveform Inversion of Ground-Penetrating Radar Data to Monitor the Water Front in Limestone, IEEE Journal of Selected Topics in Applied Earth Observations and Remote Sensing. 10 (2017) 4328–4336. doi:10.1109/JSTARS.2017.2743215.

[21] M. Chouteau, S. Vallières, E. Toe, A multi-dipole mobile array for the non-destructive evaluation of pavement and concrete infrastructures: a feasability study, in: Proceedings of the BAM International Symposium NDT-CE, Berlin, Germany, 2003: pp. 16–19.

[22] R.B. Polder, Critical chloride content for reinforced concrete and its relationship to concrete resistivity, Materials and Corrosion. 60 (2009) 623–630. doi:10.1002/maco.200905302.

[23] M. Fares, G. Villain, S. Bonnet, S. Palma Lopes, B. Thauvin, M. Thiery, Determining chloride content profiles in concrete using an electrical resistivity tomography device, Cement and Concrete Composites. 94 (2018) 315–326. doi:10.1016/j.cemconcomp.2018.08.001.

[24] K. Hornbostel, C.K. Larsen, M.R. Geiker, Relationship between concrete resistivity and corrosion rate – A literature review, Cement and Concrete Composites. 39 (2013) 60–72. doi:10.1016/j.cemconcomp.2013.03.019.

[25] A.Q. Nguyen, G. Klysz, F. Deby, J.-P. Balayssac, Evaluation of water content gradient using a new configuration of linear array four-point probe for electrical resistivity measurement, Cement and Concrete Composites. 83 (2017) 308–322. doi:10.1016/j.cemconcomp.2017.07.020.

[26] G. Villain, V. Garnier, Z.M. Sbartaï, X. Derobert, J.-P. Balayssac, Development of a calibration methodology to improve the on-site non-destructive evaluation of concrete durability indicators, Materials and Structures. 51 (2018) 40.

[27] S.E.S. Mendes, R.L.N. Oliveira, C. Cremonez, E. Pereira, E. Pereira, R.A. Medeiros-Junior, Electrical resistivity as a durability parameter for concrete design: Experimental data versus estimation by mathematical model, Construction and Building Materials. 192 (2018) 610–620. doi:10.1016/j.conbuildmat.2018.10.145.

[28] C. Rücker, T. Günther, The simulation of finite ERT electrodes using the complete electrode model, Geophysics. 76 (2011) F227–F238.

[29] K. Gowers, S. Millard, Measurement of concrete resistivity for assessment of corrosion, ACI Materials Journal. 96 (1999).

[30] F. Wenner, A method for measuring earth resistivity, Journal of the Washington Academy of Sciences. 5 (1915) 561–563.

[31] R.B. Polder, Test methods for on site measurement of resistivity of concrete — a RILEM TC-154 technical recommendation, Construction and Building Materials. 15 (2001) 125–131. doi:10.1016/S0950-0618(00)00061-1.

[32] C. Andrade, R. Polder, M. Basheer, Non-destructive methods to measure ion migration, RILEM TC. (2007) 91–112.

[33] L. Bourreau, V. Bouteiller, F. Schoefs, L. Gaillet, B. Thauvin, J. Schneider, S. Naar, Uncertainty assessment of concrete electrical resistivity measurements on a coastal bridge,

539 Structure and Infrastructure Engineering. 15 (2019) 443–453.
540 doi:10.1080/15732479.2018.1557703.
541 [34] J. Priou, Y. Lecieux, M. Chevreuil, V. Gaillard, C. Lupi, D. Leduc, E. Rozière, R. Guyard, F.
542 Schoefs, In situ DC electrical resistivity mapping performed in a reinforced concrete wharf
543 using embedded sensors, Construction and Building Materials. 211 (2019) 244–260.
544 doi:10.1016/j.conbuildmat.2019.03.152.
545 [35] L. Marescot, S. Rigobert, S.P. Lopes, R. Lagabrielle, D. Chapellier, A general approach for DC
546 apparent resistivity evaluation on arbitrarily shaped 3D structures, Journal of Applied
547 Geophysics. 60 (2006) 55–67.
548 [36] G. Kunetz, Principles of direct current-Resistivity prospecting, (1966).
549 [37] G.A. Oldenborger, P.S. Routh, M.D. Knoll, Sensitivity of electrical resistivity tomography data
550 to electrode position errors, Geophysical Journal International. 163 (2005) 1–9.
551 [38] C.-Y. Chang, S.-S. Hung, Implementing RFIC and sensor technology to measure temperature
552 and humidity inside concrete structures, Construction and Building Materials. 26 (2012) 628–
553 637.
554 [39] D. LaBrecque, W. Daily, Assessment of measurement errors for galvanic-resistivity electrodes
555 of different composition, Geophysics. 73 (2008) F55–F64.
556 [40] K. Liang, X. Zeng, X. Zhou, C. Ling, P. Wang, K. Li, S. Ya, Investigation of the capillary rise in
557 cement-based materials by using electrical resistivity measurement, Construction and Building
558 Materials. 173 (2018) 811–819.
559 [41] Y. Abbas, F. Pargar, W. Olthuis, A. van den Berg, Activated carbon as a pseudo-reference
560 electrode for potentiometric sensing inside concrete, Procedia Engineering. 87 (2014) 1437–
561 1440.
562 [42] M. Petrič, S. Kastelica, P. Mrvar, Selection of electrodes for the'in situ'electrical resistivity
563 measurements of molten aluminium, Journal of Mining and Metallurgy B: Metallurgy. 49
564 (2013) 279–283.
565 [43] O. Kuras, P.B. Wilkinson, P.I. Meldrum, R.T. Swift, S.S. Uhlemann, J.E. Chambers, F.C.
566 Walsh, J.A. Wharton, N. Atherton, Performance Assessment of Novel Electrode Materials for
567 Long-term ERT Monitoring, in: Near Surface Geoscience 2015-21st European Meeting of
568 Environmental and Engineering Geophysics, 2015.
569 [44] J. Song, L. Wang, A. Zibart, C. Koch, Corrosion protection of electrically conductive surfaces,
570 Metals. 2 (2012) 450–477.
571 [45] L.S. Edward, A modified pseudo section for resistivity and induced-polarization, Geophysics.
572 42 (1977) 1020–1036.
573 [46] M. Loke, Electrical Imaging Surveys for Environmental and Engineering Studies, 2000.
574 [47] S.K. Park, G.P. Van, Inversion of pole-pole data for 3-D resistivity structure beneath arrays of
575 electrodes, GEOPHYSICS. 56 (1991) 951–960. doi:10.1190/1.1443128.
576 [48] W.J. McCarter, H.M. Taha, B. Suryanto, G. Starrs, Two-point concrete resistivity
577 measurements: interfacial phenomena at the electrode–concrete contact zone, Measurement
578 Science and Technology. 26 (2015) 085007.
579 [49] D. Chapellier, Diagraphies appliquées à l'hydrologie, technique et documentation (Lavoisier),
580 Diagraphies, 1987.

581 [50] W. Morris, E.I. Moreno, A.A. Sagüés, Practical evaluation of resistivity of concrete in test
582 cylinders using a Wenner array probe, Cement and Concrete Research. 26 (1996) 1779–1787.
583 [51] G.E. Archie, The electrical resistivity log as an aid in determining some reservoir
584 characteristics, Transactions of the American Institute of Mining and Metallurgical Engineers.
585 (1942) 54–62.
586